Organic &
Biomolecular
Chemistry

Cite this: *Org. Biomol. Chem.*, 2011, **9**, 4256

www.rsc.org/obc

PAPER

Product selectivity control induced by using liquid–liquid parallel laminar flow in a microreactor†

Fumihiro Amemiya,[b] Hideyuki Matsumoto,[c] Keishi Fuse,[b] Tsuneo Kashiwagi,[b] Chiaki Kuroda,[c] Toshio Fuchigami[b] and Mahito Atobe*[a,b]

Received 31st January 2011, Accepted 17th March 2011
DOI: 10.1039/c1ob05174a

Product selectivity control based on a liquid–liquid parallel laminar flow has been successfully demonstrated by using a microreactor. Our electrochemical microreactor system enables regioselective cross-coupling reaction of aldehyde with allylic chloride *via* chemoselective cathodic reduction of substrate by the combined use of suitable flow mode and corresponding cathode material. The formation of liquid–liquid parallel laminar flow in the microreactor was supported by the estimation of benzaldehyde diffusion coefficient and computational fluid dynamics simulation. The diffusion coefficient for benzaldehyde in Bu_4NClO_4-HMPA medium was determined to be 1.32×10^{-7} cm^2 s^{-1} by electrochemical measurements, and the flow simulation using this value revealed the formation of clear concentration gradient of benzaldehyde in the microreactor channel over a specific channel length. In addition, the necessity of the liquid–liquid parallel laminar flow was confirmed by flow mode experiments.

Introduction

In synthetic chemistry, the control of product selectivity has always been an important subject. Product selectivity can be defined as the ratio of the desired product to all products in a chemical reaction which gives a mixture of desired product and some by-products. Since a simple process with high product selectivity is required especially in an industrial production, considerable efforts have been spent for the development of a novel method or strategy for product selectivity control.

Product selectivity is usually controlled by chemical factors such as steric effect, resonance effect, solvent effect, amount of reactant, and electron orbital interaction. They induce intentional changes of transition state stability or intermediate stability of the reaction molecule(s) during a reaction. On the other hand, novel type of strategies have also been developed recently. For example, ultrasonic irradiation,[1] microwave irradiation,[2] site-isolation,[3] and continuous flow systems[4] have been reported to control the product selectivity of a reaction. In these cases, the use of unique external circumstances of a reaction induces the specific change of reaction route or reaction pattern without adding special reactants or catalysts.

Micro-flow systems (microreactor or micromixer system) have also enabled product selectivity control.[5] In micro-flow systems, the product selectivity of a reaction can be significantly improved due to the extremely fast and efficient mixing and heat transfer stemming from small size and high surface-to-volume ratio of microstructures. On the basis of these advantages, Yoshida and his coworkers have successfully demonstrated selective formations of desired products using highly reactive intermediates by micro-flow systems. They further propose a concept of *space integration* for fast and selective chemical synthesis by using flow microreactor systems.[6]

Recently, we have also reported a novel type of strategy for product selectivity control using an electrochemical micro-reactor.[7] This system employed cathodic carbonyl allylation as a model reaction.[8] This reaction provides two regioisomeric products such as γ- and α-adducts by specific way. Tokuda *et al.* clarified that the regioselectivity of these products was mainly related to the difference in the reduction potentials between the two starting substrates, although the regioselectivity of this reaction is also influenced by electrode materials, the concentration of supporting electrolytes and current density.[9] In other words, electrochemical carbonyl allylation can produce either γ- or α-adducts depending on whether the aldehyde or allylic halide is reduced by the cathode. If the aldehyde has a higher reduction potential, the allylic halide is predominantly reduced to give the γ-adduct but if the reduction potential of the allylic halide is higher, the aldehyde is reduced preferentially and the α-adduct generation is favored. Therefore,

---

[a] *Department of Environment and System Sciences, Yokohama National University, 79-7 Tokiwadai, Hodogaya-ku, Yokohama, 2408501, Japan. E-mail: atobe@ynu.ac.jp; Fax: +81 45 339 4214; Tel: +81 45 339 4214*

[b] *Department of Electronic Chemistry, Tokyo Institute of Technology, 4259 Nagatsuta-cho, Midori-ku, Yokohama, 2268502, Japan*

[c] *Department of Chemical Engineering, Tokyo Institute of Technology, 2-12-1 Ookayama, Meguro-ku, Tokyo, 1528550, Japan*

† Electronic supplementary information (ESI) available. See DOI: 10.1039/c1ob05174a

control of the product selectivity (regioselectivity in this reaction) requires that either the allylic halides or aldehydes should be reduced chemoselectively, regardless of their reduction potentials (Scheme 1).

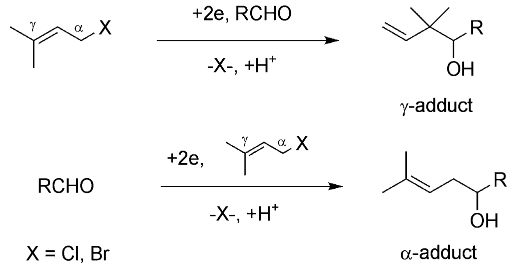

Scheme 1 The reaction pathway of cathodic carbonyl allylation between an allylic halide and an aldehyde.

To perform chemoselective cathodic reduction, we employed a liquid–liquid parallel laminar flow formed in an electrochemical microreactor. The channel of the microreactor is sufficiently small to ensure stable and laminar flow of solutions. As shown in Fig. 1, when two solutions (allylic chloride solution and aldehyde solution) are introduced through respective inlets (inlet 1 and inlet 2) of the microreactor, a stable liquid–liquid interface can be formed, and mass transfer between the input streams occurs only by means of diffusion. Therefore, the substrate introduced through inlet 1 (inflow 1) could be predominantly reduced, whereas the reduction of the inlet 2 substrate (inflow 2) could be avoided. Consequently, chemoselective cathodic reduction would proceed and an intentional cross-coupling product would be obtained regioselectively. In other words, product selectivity control would be realized by simply switching the reagent flows. The system applied this strategy can be also regarded as one of the practical example of space integration.

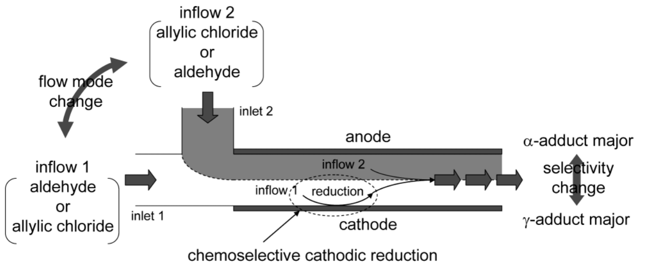

Fig. 1 Product selectivity control in cathodic carbonyl allylation using a parallel laminar flow in the microreactor. The substrate of inflow 1 is selectively reduced at the cathode to give the desired product as major product.

The successful preliminary results prompted us to perform a further systematic study of the product selectivity control based on liquid–liquid parallel laminar flow in the microreactor. Herein, we wish to report the full details of our study. The formation of liquid–liquid parallel laminar flow in the microreactor channel was especially focused so that our concept was verified to work.

Results and discussion

First of all, in order to confirm that substrate was prevented from reaching the counter electrode surface by the use of liquid–liquid parallel laminar flow, cyclic voltammograms (CVs) were measured for the reduction of benzaldehyde (**2a**) in the microreactor. A reduction peak of **2a**, as shown in Fig. 2(b), was clearly observed at −1.89 V *vs.* Ag wire when an electrolytic stream containing **2a** entered only through inlet 1 of Fig. 1 (cathode side inlet). On the other hand, the peak current was significantly decreased when an electrolytic solution with **2a** was introduced through inlet 2 (anode side inlet), and a solution without **2a** was introduced through inlet 1 (Fig. 2(c)). This result indicated that the use of liquid–liquid parallel laminar flow did prevent **2a** from reaching the cathode when it was introduced through inlet 2.

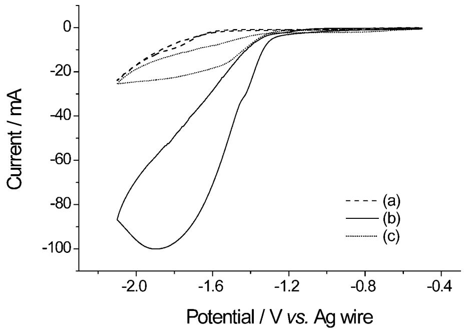

Fig. 2 Cyclic voltammograms for the reduction of benzaldehyde (**2a**) in 200 mM n-Bu_4NClO_4-hexamethylphosphoric triamide (HMPA) using a microreactor with a Pt cathode. Ag wire as a reference electrode was placed externally, downstream near the outlet of the microreactor. The scan rate was 100 mV s^{-1}. (a) HMPA solution without **2a** was introduced through inlet 1 of Fig. 1 at a flow rate of 0.02 mL min^{-1} (background). (b) HMPA solution with **2a** (1 M) was introduced through inlet 1 at a flow rate of 0.02 mL min^{-1}. (c) HMPA solution with **2a** (2 M) was introduced through inlet 2, and HMPA solution without **2a** was introduced through inlet 1, both at a flow rate of 0.01 mL min^{-1}.

Next, reduction potentials of substrates were measured by cyclic voltammetry in 0.2 M n-Bu_4NClO_4/hexamethylphosphoric triamide (HMPA) medium recorded at (a) platinum (Pt), (b) glassy carbon (GC), and (c) silver (Ag) electrodes. As shown in Fig. 3(a),

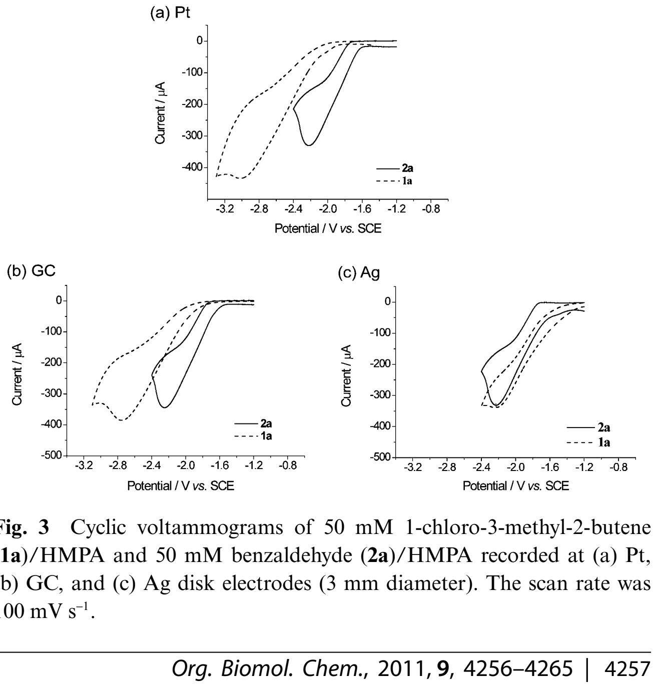

Fig. 3 Cyclic voltammograms of 50 mM 1-chloro-3-methyl-2-butene (**1a**)/HMPA and 50 mM benzaldehyde (**2a**)/HMPA recorded at (a) Pt, (b) GC, and (c) Ag disk electrodes (3 mm diameter). The scan rate was 100 mV s^{-1}.

2a was reduced at *ca.* –2.22 V *vs.* SCE (peak potential), while 1-chloro-3-methyl-2-butene (**1a**) was reduced at *ca.* 3.02 V *vs.* SCE at the Pt electrode. As mentioned in the above, the regioselectivity of this model reaction is mainly influenced by the difference in the reduction potentials between two starting substrates. When aldehydes are more readily reduced than allylic halides, the reduction yields α-adducts preferentially. Thus, it can be predicted that the α-adduct would be obtained as a major product at the bulk electrolysis using a Pt electrode. From the result of Fig. 3(b), GC electrode would also show similar product selectivity. On the other hand, as shown in Fig. 3(c), **1a** and **2a** were reduced at almost same potentials (*ca.* –2.23 V *vs.* SCE) at the Ag electrode. This was ascribed to a electrocatalytic activity of Ag electrode for the reduction of organic halides.[10] Therefore, it is expected that a nearly equal amount of γ-adduct and α-adduct are obtained at the bulk electrolysis using an Ag electrode.

Subsequently, preparative experiments of the cathodic cross-coupling reaction were carried out using **1a** and **2a** substrate combination. Since the reduction potential of **2a** is much lower than that of **1a** at the Pt electrode, α-adduct was obtained as a major product when the reaction was carried out using a conventional batch type reactor with the Pt cathode (Table 1, entry 1). Similar results were obtained by using the microreactor with single flow mode (see. the figure of Table 1) and the Pt and GC cathodes (entry 2 and entry 3). In contrast, as shown in entry 4, the yield of γ-adduct was increased by using the Ag electrode. These experimental results well reflected the results of CVs in Fig. 2. Then, in order to improve the γ-adduct selectivity, 1-bromo-3-methyl-2-butene (**1b**) was used instead of **1a** in entry 5 because **1b** has lower reduction potential than that of **1a**. However, the total yield was significantly decreased though γ-adduct was obtained dominantly. In this case, bromide ion derived cathodically from **1b** would be oxidized at the anode to give Br^+ species (Br^+, Br_3^-, Br_2, *etc.*), and then, they were reduced at the cathode to regenerate bromide ion. Thus, a large part of the electricity seemed to be consumed for the redox reaction of Br^-/Br^+. In fact, the electrolyte solution collected in a vessel after the electrolysis showed bright yellow color and the color turned light brown after several hours. It should be noted that chloride ion has higher oxidation potential than that of bromide ion and anodically generated Cl_2 would be removed to gas phase. Therefore, the system would be less affected by the redox reaction of Cl^-/Cl^+ than that of Br^-/Br^+. As shown in entry 6, the selectivity of α-adduct was improved by using the microreactor with the flow mode (a). The 90% of substrate **1a** was converted in this condition, however, hydrobenzoin, benzyl alcohol and homo-coupling products of **1a** were also detected as by-products. (The oxidation of HMPA occurred simultaneously in the anode because HMPA has a lower oxidation potential.) Since these homo-coupling side-reactions would occur simultaneously in entry 6, the yield was improved by decreasing the concentration of **2a** as shown in entry 7. (The current efficiency for **4a** was 27.1% and the productivity was 26.8 mg h^{-1}.) On the other hand, the use of the flow mode (b) significantly increased the γ-adduct selectivity (entry 8). These results indicated that our concept for chemoselective cathodic reduction by using a parallel laminar flow in the microreactor works. As shown in entry 9, the use of the Ag electrode with flow mode (a) couldn't enhance α-adduct selectivity compared to the result in entry 4. However, the selectivity was reversed and γ-adduct was obtained as a major product when the electrolysis was performed by a combination use of the Ag electrode and flow mode (b) (entry 10, the current efficiency for **3a** was 33.4% and the productivity was 32.9 mg h^{-1}). It should be noted that this was opposite selectivity compared to that obtained in entry 7.

Table 1 Cathodic carbonyl allylation between **1a** and **2a** using the microreactor[a]

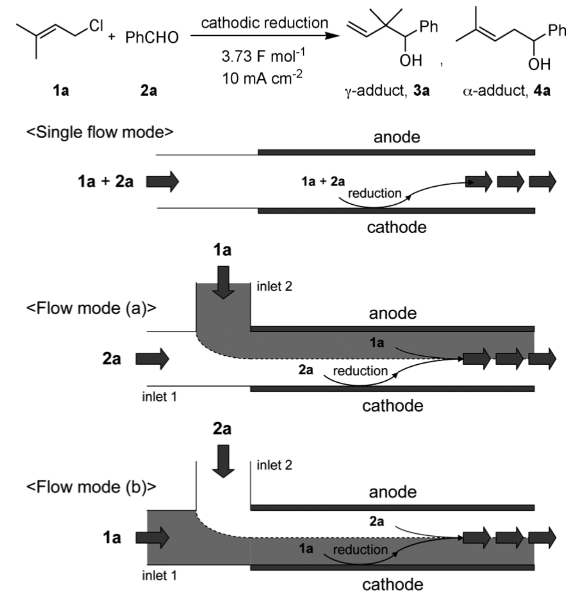

Entry	Cathode material	Flow mode	Total yield (%)[b] **3a** + **4a**	Selectivity[b] **3a** : **4a**
1[c]	Pt	Batch type reactor	69	29 : 71
2	Pt	Single flow mode	64	17 : 83
3	GC	Single flow mode	54	15 : 85
4	Ag	Single flow mode	63	45 : 55
5[d]	Ag	Single flow mode	10	>99 : <1
6	Pt	Flow mode (a)	44	9 : 91
7[e]	Pt	Flow mode (a)	55	8 : 92
8	Pt	Flow mode (b)	58	41 : 59
9	Ag	Flow mode (a)	60	47 : 53
10	Ag	Flow mode (b)	75 (67)[f]	87 : 13

[a] Experimental conditions: The concentration of **1a** in HMPA was 500 mM, and that for **2a** was 2 M. *n*-Bu_4NClO_4 was used as a supporting electrolyte in all solutions (200 mM). Flow rates of each solution were 0.01 mL min^{-1} and the total flow rate was 0.02 mL min^{-1}. All reactions were performed at 0 °C. [b] Determined by GC analysis. [c] Reported in the literature.[9] [d] 1-Bromo-3-methyl-2-butene (**1b**) was used instead of **1a**. [e] The concentration of **2a** was 1 M. [f] Isolated yield in parenthesis.

In addition to the above experiments, it is important to verify the formation of liquid–liquid parallel laminar flow in the microreactor channel and the substrate diffusion behavior in such a flow mode. Therefore, the diffusion coefficient for **2a** in HMPA medium was then estimated and the spatial distribution of the substrate in the microreactor was investigated by computational fluid dynamics (CFD) simulation. Under the experimental conditions used in this study, the simulation was carried out using different diffusion coefficients for **2a** (D_{BA}) in the range from 5×10^{-6} to 1×10^{-8} cm^2 s^{-1}. This range of diffusion coefficient roughly covers from the diffusion of general small organic molecules in the low viscosity solvent to their diffusion in high viscosity medium such as ionic liquids. For example, the diffusion coefficient for ferrocene

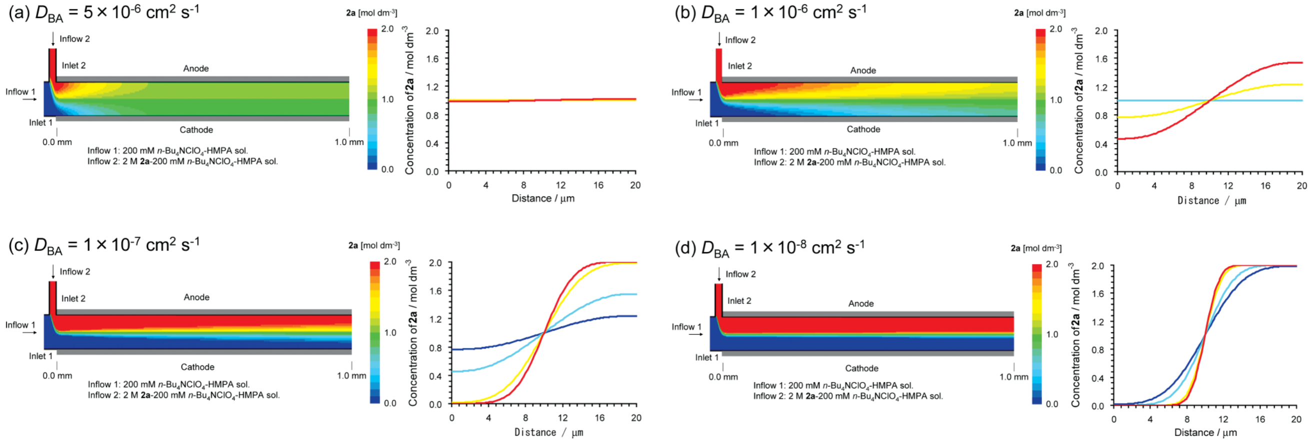

Fig. 4 Schematic visualizations of the CFD simulation results for **2a** diffusion in the microreactor channel from inlets to 1.0 mm down stream position and corresponding **2a** concentration distribution curves at the specific positions. Each flow rate was fixed at 0.01 mL min^{-1}. The electrode distance was set as 20 μm. In the CFD visualizations, the vertical scale is different from the horizontal scale. Both two inlets have 20 μm width. In the distribution curves, the x axis shows the distance from the cathode surface. Red, yellow, light blue, and blue curves show the distributions at 0.5, 1, 5, and 10 mm down stream positions from inlets, respectively. (a) D_{BA} was set as 5 × 10^{-6} cm^2 s^{-1}. (b) D_{BA} was set as 1 × 10^{-6} cm^2 s^{-1}. (c) D_{BA} was set as 1 × 10^{-7} cm^2 s^{-1}. (d) D_{BA} was set as 1 × 10^{-8} cm^2 s^{-1}.

in acetonitrile (η = 0.345 × 10^{-4} Pa s)[11] was estimated as 2.3 × 10^{-5} cm^2 s^{-1},[12] while the value for methyl viologen in a typical ionic liquid 1-n-butyl-3-methylimidazolium hexafluorophosphate ([bmim][PF$_6$], η = 2.33 × 10^{-1} Pa s)[13] was estimated as 1.1 × 10^{-8} cm^2 s^{-1} [14] Fig. 4 shows schematic visualizations of the CFD simulation results for **2a** diffusion in the microreactor channel from inlets to 1.0 mm down stream position and corresponding **2a** concentration distribution curves at the specific positions. In Fig. 4(a), when D_{BA} was set as 5 × 10^{-6} cm^2 s^{-1}, **2a** immediately diffused to the cathode surface and the input streams were completely mixed each other even at 1 mm down stream position. This tendency was not significantly improved when D_{BA} was set as 1 × 10^{-6} cm^2 s^{-1}, as shown in Fig. 4(b). In contrast, when D_{BA} was set as 1 × 10^{-7} cm^2 s^{-1}, the concentration gradient clearly remained even at 1 cm down stream position, as shown in Fig. 4(c). In this case, the concentration of **2a** on the cathode surface was diluted especially in the former part of the cell. Furthermore, the concentration distribution was drastically changed in the order of 10^{-8} cm^2 s^{-1}. In this order of D_{BA} value, **2a** hardly diffuse to the cathode surface and the concentration of **2a** on the cathode surface is extremely low (Fig. 4(d)). The resulting **2a** concentration profiles are qualitatively in agreement with the CV results obtained in Fig. 2. Therefore, it can be assumed that the real D_{BA} value in the n-Bu$_4$NClO$_4$-HMPA medium would be found in the range from 1 × 10^{-8} to 1 × 10^{-7} cm^2 s^{-1}.

Subsequently, in order to estimate D_{BA} value, Wilke–Chang equation was employed. Wilke–Chang equation, which is a modified form of Stokes–Einstein equation obtained experimentally, is probably the most widely used to estimate diffusion coefficient in liquid phase systems.[15] The equation is:

$$D_{BA} = 7.4\times10^{-8}\frac{(\varphi M_{sol})^{1/2}T}{\eta_{sol}V_{BA}} \tag{1}$$

where φ is the association factor of solvent, M_{sol} is the molecular weight of solvent, T is the absolute temperature, η_{sol} is the viscosity of solvent, and V_{BA} is the molal volume of **2a** at its normal boiling temperature. M_{sol} of HMPA is 179.20 g mol^{-1}. T was set as 273.15 K (0 °C) in this system. φ was set as 0.7 which the value is derived from the association factor of aromatic hydrocarbon. To obtain the η_{sol} value, the rheology of n-Bu$_4$NClO$_4$-HMPA medium was measured experimentally. Fig. 5 shows the relationships between shear rate (γ) and shear stress (τ) of three samples (sample A: 200 mM n-Bu$_4$NClO$_4$-HMPA sol., sample B: 1 M **2a**-200 mM n-Bu$_4$NClO$_4$-HMPA sol., sample C: 2 M **2a**-200 mM n-Bu$_4$NClO$_4$-HMPA sol.) at 0 °C. Linear relationships were observed in each sample, suggesting that these media are Newtonian fluids. Thus, the viscosity (μ) of these samples was estimated by following equation:

$$\tau = \mu\gamma \tag{2}$$

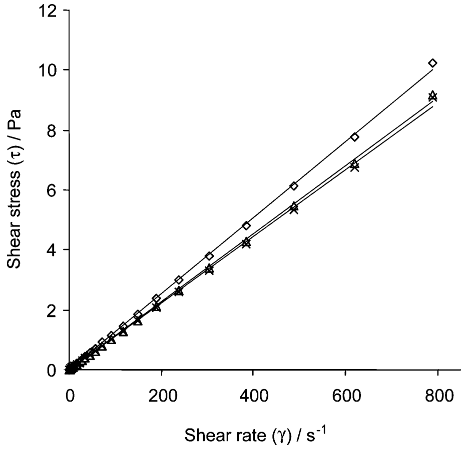

Fig. 5 The relationships between shear rate (γ) and shear stress (τ) of n-Bu$_4$NClO$_4$-HMPA mediums recorded by a rheometer at 0 °C. Rhombic plots: sample A, 200 mM n-Bu$_4$NClO$_4$-HMPA sol., τ/γ = 1.27 × 10^{-2} Pa s. Triangle plots: sample B, 1 M **2a**-200 mM n-Bu$_4$NClO$_4$-HMPA sol., τ/γ = 1.13 × 10^{-2} Pa s. X shape plots: sample C, 2 M **2a**-200 mM n-Bu$_4$NClO$_4$-HMPA sol., τ/γ = 1.11 × 10^{-2} Pa s. Plots are average values of three times measurements.

and determined to be 1.27 × 10^{-2}, 1.13 × 10^{-2} and 1.11 × 10^{-2} Pa s for samples A, B and C, respectively. These results suggest that the concentration of **2a** slightly affects their viscosity. The viscosity of sample A (1.27 × 10^{-2} Pa s) was employed as $\eta_{\rm sol}$ in eqn (1). The molal volume of **2a** at normal boiling point ($V_{\rm BA}$) was estimated by Le Bas method.[16] The molecular formula of **2a** is C_7H_6O, and additive volumes of carbon atom, hydrogen atom, oxygen atom, and ring structure are 14.8, 3.7, 7.4, −15.0 $\rm cm^3\ g^{-1}\ mol^{-1}$, respectively. Therefore, the $V_{\rm BA}$ value was determined to be 118.2 $\rm cm^3\ g^{-1}\ mol^{-1}$. Consequently, by using eqn (1) with these values, $D_{\rm BA}$ was estimated as 1.02×10^{-6} $\rm cm^2\ s^{-1}$.

This $D_{\rm BA}$ value is far different from the value expected by CV results and CFD simulations. This may be attributed to the following reasons: (i) Wilke–Chang equation is supposed to estimate at very low concentration of solute condition, not suited for extremely high concentration condition like 2 M. (ii) Wilke–Chang equation would not be applied for the estimation in high viscosity medium like 1.27×10^{-2} Pa s. (iii) The association factor of HMPA (φ) would be significantly different from the real value. Hence, it is rather difficult to estimate the precise $D_{\rm BA}$ value in the n-$\rm Bu_4NClO_4$-HMPA medium by using prediction equations.

Thus, in the next step, $D_{\rm BA}$ was measured experimentally by potential step chronoamperometry and steady-state cyclic voltammetry. Although there are several methods for measuring molecular diffusion coefficient in a solution such as optical scattering measurement[17] and NMR spectrometry,[18] the electrochemical measurements have some advantages because they can be carried out by using common apparatus with short experimental time. This method needs fast electron transfer between an electrode and target molecules, and the use of adequate amount of supporting electrolyte is inevitable. Initially, to determine $D_{\rm BA}$ value and the number of electrons (n) for the **2a** reduction, the potential step chronoamperometry was performed using 10 mM **2a**/0.2 M n-$\rm Bu_4NClO_4$-HMPA solution with a sample time of 0.001 s recorded at the Pt disk electrode (3 mm diameter). The sample was pretreated by holding the potential at a point corresponding to zero faradaic current (0.00 V *vs*. SCE) for 2 s, after which the potential was stepped to a potential higher than the **2a** reduction peak potential (−2.6 V *vs*. SCE) and the current measured for 10 s at 0 °C. The time-dependent current response obtained at the first step was showed in Fig. 6 and corresponding Cottrell plot was inserted in the figure (the Cottrell plot was corrected by subtraction of the background current.). The current was almost linear with the reciprocal of the square root of time from 2.23 to 0.31 $\rm s^{-1/2}$. The relationship between $D_{\rm BA}$ and n was then obtained by fitting to the following Cottrell equation:

$$I = \frac{nFAD_{\rm BA}c}{(\pi D_{\rm BA}t)^{1/2}} = 9.82 \times 10^{-5} t^{-1/2} \tag{3}$$

where, I, F, A and c are the current, the Faraday constant, the geometric surface area of the working electrode, and the concentration of **2a**, respectively.

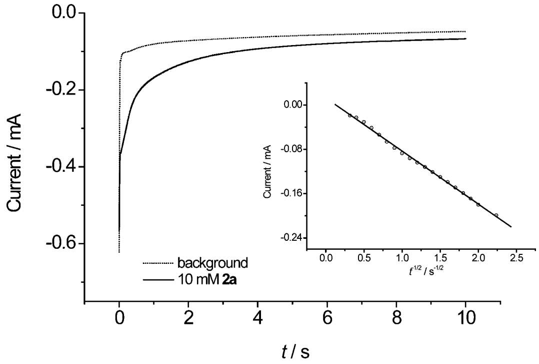

Fig. 6 Potential step chronoamperogram for the reduction of 10 mM **2a** in HMPA containing 0.2 M n-$\rm Bu_4NClO_4$ recorded at the Pt disk electrode at 0 °C. The potential was stepped from 0.0 to −2.6 V *vs*. SCE. The corresponding Cottrell plot was inserted in the figure.

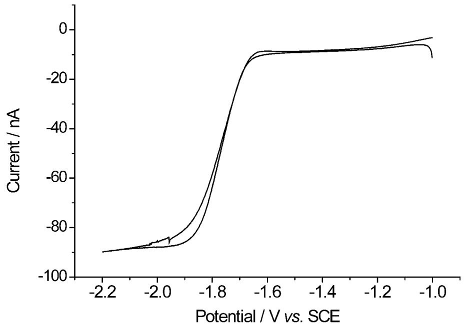

Fig. 7 Steady-state cyclic voltammogram for the reduction of 10 mM **2a** at the Pt micro disk electrode (100 μm diameter) in 0.2 M n-$\rm Bu_4NClO_4$-HMPA solution at 0 °C. The scan rate was 10 mV $\rm s^{-1}$.

To determine $D_{\rm BA}$ and n values, another relationship between $D_{\rm BA}$ and n was estimated by steady-state cyclic voltammetry using a Pt micro disk electrode (100 μm diameter) with a slow scan rate. Fig. 7 shows the CV for the reduction of 10 mM **2a** in 0.2 M n-$\rm Bu_4NClO_4$-HMPA solution recorded at 0 °C, and the measured diffusion limiting current was obtained as 7.63 × 10^{-8} A (This limiting current was corrected by subtraction of the background current.). Thus, the relationship between $D_{\rm BA}$ and n was obtained by fitting to the following equation:

$$I_{\rm lim} = 4nFcD_{\rm BA}a = 7.63 \times 10^{-8}\ {\rm A} \tag{4}$$

where a is the radius of the micro disk electrode. Then, from the simultaneous equations of eqn (3) and (4), $D_{\rm BA}$ and n were determined to be 2.40 × 10^{-6} $\rm cm^2\ s^{-1}$ and 1.65, respectively. This n value suggests that the reduction mechanism should be a concerted reaction involving 1e and 2e reductions. Actually, a small amount of homo-coupling product (pinacol) was detected as a 1e reduction by-product. The desired coupling products were usually obtained in approximately 60% total yield as 2e reduction products. These facts support the concerted reaction mechanism involving 40% of 1e reduction and 60% of 2e reduction (the n value should be 1.60 in this case). On the other hand, this $D_{\rm BA}$ value is close to that obtained by Wilke–Chang equation, suggesting that such estimation can be successfully applied under the low **2a** concentration condition. Nevertheless, the real $D_{\rm BA}$ value under high concentration condition (2 M **2a**) is still not confirmed. Thus, subsequently, additional steady-state cyclic voltammetry was carried out for the reduction of 2 M **2a** in 0.2 M n-$\rm Bu_4NClO_4$-HMPA solution at 0 °C. As shown in Fig. 8, the diffusion limiting current was obtained as 2.10 × 10^{-8} A. Then, by using n value of 1.65 obtained in the above and the following equation:

$$I_{\rm lim} = 4 \times 1.65 \times FcD_{\rm BA}a = 2.10 \times 10^{-8}\ {\rm A} \tag{5}$$

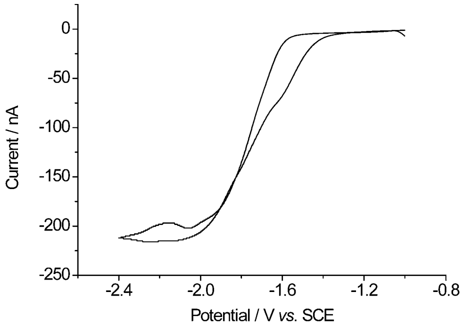

Fig. 8 Steady-state cyclic voltammogram for the reduction of 2 M **2a** at the Pt micro disk electrode (25 μm diameter) in 0.2 M n-Bu_4NClO_4-HMPA solution at 0 °C. The scan rate was 10 mV s^{-1}.

the real D_{BA} value under the high concentration condition (2 M **2a**) was determined to be 1.32×10^{-7} cm^2 s^{-1}. This D_{BA} value is approximately one order of magnitude lower than that under the low concentration condition, indicating that the concentration of **2a** greatly affects their D_{BA} values and the diffusion manner of liquid–liquid parallel laminar flow in the microreactor channel.

Fig. 9 show computational simulation result of liquid–liquid parallel laminar flow in the microreactor channel using the D_{BA} value obtained by eqn (5). The result of this CFD simulation clearly supports the formation of concentration gradient of substrate in the microreactor channel over a specific length. However, the electrochemically measured D_{BA} value was little larger than the predicted value. As stated in the above, the CFD simulations using several orders of diffusion coefficient suggest that D_{BA} value would be found in the range from 1×10^{-8} to 1×10^{-7} cm^2 s^{-1}. This minor difference between the predicted D_{BA} value and measured D_{BA} value would indicate that some unknown factors may affect and disturb the **2a** diffusion in the microreactor channel. Actually, a decrease of molecular diffusion in micro-nano channels have been observed in the literature.[19] This phenomenon can be attributed to the increased number of interactions between medium and the channel walls, which can no longer be neglected when the channel size reaches a critical value. Therefore, it might be possible that such interactions reduce the D_{BA} value and the clear concentration gradient of **2a** is kept in the microreactor channel. Hence, it might be necessary for more accurate simulation to combine a new diffusion model, considering an interaction between substrate and wall, with macro-scale models, which were based on Navier–Stokes equations and species transport equations.

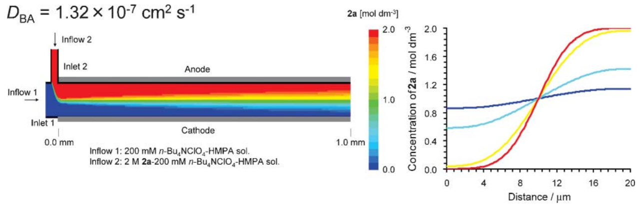

Fig. 9 Schematic visualization of the CFD simulation result for **2a** diffusion in the microreactor channel from inlets to 1.0 mm down stream position and corresponding **2a** concentration distribution curves at the specific positions. Each flow rate was fixed at 0.01 mL min^{-1}. The electrode distance was set as 20 μm. In the CFD visualization, the vertical scale is different from the horizontal scale. Both two inlets have 20 μm width. In the distribution curves, the x axis shows the distance from the cathode surface. Red, yellow, light blue, and blue curves show the distributions at 0.5, 1, 5, and 10 mm down stream positions from inlets, respectively. D_{BA} was set as 1.32×10^{-7} cm^2 s^{-1}.

Next, the necessity of the liquid–liquid parallel laminar flow mode was investigated experimentally. In this cross-coupling reaction, the key step for product selectivity determination is the initial cathodic reduction. If the cathodically generated intermediate can be transferred to the outlet of the electrochemical microreactor without its decomposition or conversion to undesired byproducts, a flow mode illustrated in Fig. 10(b), in which an electrolytic solution containing another substrate is introduced at the outlet of the electrochemical microreactor, would be also useful for the effective control of product selectivity. In practice, however, the desired cross-coupling reaction was not proceeded at all. This is ascribed to the fact that the stability of the reactive intermediate generated at the cathode was insufficient to transfer it to the outlet of the reactor without decomposition or side-reactions. In contrast, in the liquid–liquid parallel laminar flow mode, the reactive intermediate can be effectively trapped by another substrate before it is lost (Fig. 10(a)). Therefore, it can be stated that the liquid–liquid parallel laminar flow mode is essentially required for an efficient product selectivity control in the cross-coupling reaction.

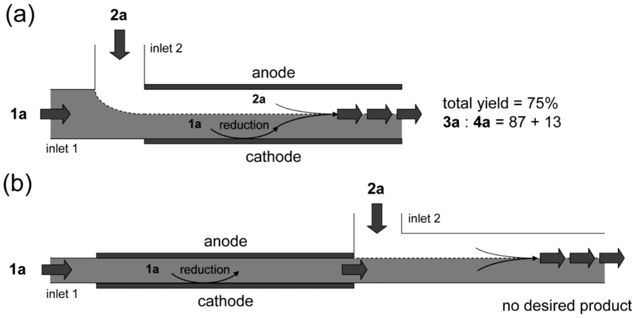

Fig. 10 Schematic illustration of two kinds of flow modes for the microreactor and their application to the cathodic cross-coupling reaction of **1a** with **2a** at the Ag cathode. (a) Liquid–liquid parallel laminar flow mode in an electric field. (b) Single laminar flow mode in an electric field. The flow rates of two electrolytic solutions containing **1a** (500 mM) and **2a** (2 M), respectively, were fixed at 0.01 mL min^{-1} each. Current density was 10 mA cm^{-2}. All reactions were performed at 0 °C.

Finally, the versatility of this microreactor system was investigated by cathodic cross-coupling reactions between **1a** and various aldehydes (**2b–e**). Before the electrolyses using the microreactor, reduction potentials of aldehydes were measured by cyclic voltammetry using the Pt disk electrode. As results, the reduction peak potentials were found to range from *ca.* −1.76 V to −2.51 V *vs.* SCE (Fig. 11). Note that the reduction peak of **1a** was observed at *ca.* −3.02 V at the Pt electrode (Fig. 3(a)). Then, cathodic cross-coupling reactions between **1a** and aldehydes (**2b–e**) were carried out using the microreactor with flow mode (a) or flow mode (b) of figures in Table 1. As results, the use of the Pt cathode with flow mode (a) provided the corresponding α-adducts as major products in reasonable yields (Table 2, entries 1, 3, 5, and 7). In this flow mode, selectivities were not affected by the reduction potentials of all aldehydes. This may be ascribed to the fact that the reduction potentials of aldehydes were lower than that of **1a** enough to reduce aldehydes chemoselectively in any case. On the other hand, the use

Table 2 Cathodic carbonyl allylation of various aldehydes using the microreactor[a]

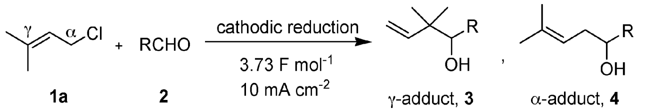

Entry	RCHO ($E_{p,red}$)[b]	Cathode material, flow mode[c]	Products 3, 4		Total yield (%)[d] 3 + 4	Selectivity[d] 3 : 4
1	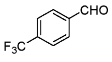 **2b** (-1.76 V)	Pt, flow mode (a)	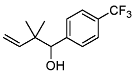 **3b**	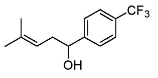 **4b**	63	15 : 85
2		Ag, flow mode (b)			65	60 : 40
3	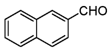 **2c** (-2.05 V)	Pt, flow mode (a)	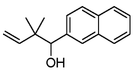 **3c**	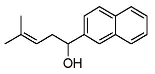 **4c**	59	12 : 88
4		Ag, flow mode (b)			54	67 : 33
5	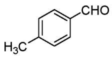 **2d** (-2.28V)	Pt, flow mode (a)	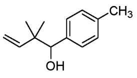 **3d**	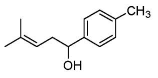 **4d**	67	10 : 90
6		Ag, flow mode (b)			68	74 : 26
7	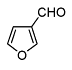 **2e** (-2.51 V)	Pt, flow mode (a)	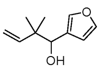 **3e**	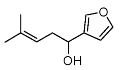 **4e**	52	19 : 81
8		Ag, flow mode (b)			49	86 : 14

[a] Experimental conditions are described in footnote *a* of Table 1. [b] Reduction peak potentials were recorded at the Pt disk electrode (Fig. 11). [c] Flow mode (a) is the flow mode for the selective reduction of aldehyde and flow mode (b) is the flow mode for the selective reduction of **1a**, as shown in the figures in Table 1. [d] Determined by ^{1}H-NMR analysis using nitromethane as an internal standard.

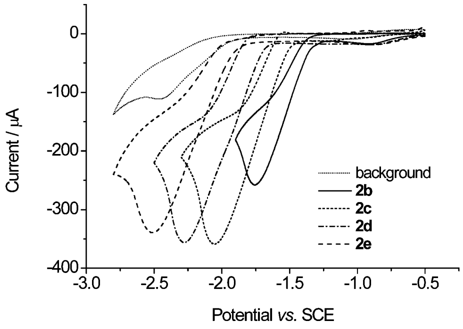

Fig. 11 Cyclic voltammograms of 50 mM aldehydes (4-(trifluoromethyl) benzaldehyde (**2b**), 2-naphthaldehyde (**2c**), *p*-tolualdehyde (**2d**) and 3-furaldehyde (**2e**)) in HMPA solution containing 200 mM n-Bu$_4$NClO$_4$ recorded at the Pt disk electrode (3 mm diameter). Scan rate was 100 mV s^{-1}.

of the Ag cathode with flow mode (b) afforded the corresponding γ-adducts as major products in good to moderate yields (entries 2, 4, 6, and 8). In this case, selectivities were slightly depended on the reduction potentials of aldehydes. Since the reduction peak of **1a** at the Ag cathode was observed at *ca.* −2.23 V (Fig. 3(c)), **1a** would be more readily reduced than **2d** or **2e**. Therefore, the reduction priority would change from aldehydes (**2d** and **2e**) to **1a** in these cases, and consequently, γ-adduct selectivity got better. From these experiments, it can be concluded that this microreactor system enables chemoselective reduction and intentional product selectivity control (regioselectivity control) in the cathodic cross-coupling reaction between allylic chloride and a wide range of aldehydes.

Conclusions

Intentional chemoselective reduction in a cathodic cross-coupling reaction was successfully carried out by using a liquid–liquid parallel laminar flow in the microreactor. The combined use of suitable flow mode and corresponding cathode material enabled control of the product selectivity (regioselectivity) in this reaction (γ-adduct/α-adduct = 8/92 in the case of flow mode (a) with Pt cathode, and γ-adduct/α-adduct = 87/13 in the case of flow mode (b) with Ag cathode in the reaction of 1-chloro-3-methyl-2-butene with benzaldehyde). The formation of liquid–liquid parallel laminar flow in the microreactor was supported by the estimation of substrate diffusion coefficient and CFD simulations. The diffusion coefficient for benzaldehyde in 200 mM n-Bu$_4$NClO$_4$-HMPA medium was determined to be 1.32×10^{-7} cm^2 s^{-1} experimentally, and the flow simulation using this value revealed the formation and stability of the concentration gradient of a substrate in the microreactor channel over a specific channel length although the simulation was not completely reflected the results of CV experiments. Besides, the necessity of the liquid–liquid parallel laminar flow mode was confirmed by flow mode experiments. This strategy serves as one of the solution for product selectivity control without adding any reactants or catalysts in a electrochemical cross-coupling reaction. Therefore, it can be expected that the present observations open a new aspect of product selectivity control using microreactor systems.

Experimental

Instrumentation

Cyclic voltammetry and chronoamperometry were performed by using a computer-controlled electrochemical analyzer (ALS/CH Instruments 630C). Preparative electrolyses were carried out with a HOKUTO DENKO HA-501 Potentiostat/Galvanostat. GC analyses were performed with a Shimadzu GC-2014 gas chromatograph with Tween 80 (2 m column). Nuclear magnetic resonance (^{1}H NMR, ^{13}C NMR) spectra were measured on JEOL JNM EX-270 spectrometer operating at 270 MHz (^{1}H NMR), 67.8 MHz (^{13}C NMR) in $CDCl_3$. All ^{1}H NMR chemical shifts were analyzed in ppm relative to internal references of TMS at δ 0.00. All ^{13}C NMR chemical shifts were analyzed in ppm relative to carbon resonance in chloroform-d$_1$ at δ 77.00. EI mass spectra were measured with a Shimadzu GCMS-QP5050A mass spectrometer. Computational fluid dynamics (CFD) simulations for liquid–liquid parallel laminar flow in the microreactor were carried out by using commercial CFD package Fluent 6.3 (ANSYS Inc.).

Materials

1-Chloro-3-methyl-2-butene (**1a**) was purchased from Aldrich and purified by distillation before use. Hexamethylphosphoric triamide (HMPA), tetrabutylammonium perchlorate (n-Bu_4NClO_4), benzaldehyde (**2a**), 4-(trifluoromethyl)benzaldehyde (**2b**), 2-naphthaldehyde (**2c**), *p*-tolualdehyde (**2d**) and 3-furaldehyde (**2e**) were purchased from Tokyo Chemical Industry and used as received.

Microreactor

Fig. 12 shows schematic illustration of the microreactor. The microreactor consisted of two plates. Each plate was glued the electrode plate (cathode plate (Pt or Ag, Nilaco) or anode plate (graphite, IGS-743, Nippon Techno-Carbon), 3 cm width, 3 cm length) and glass plate (2.6 cm width, 3 cm length) together. A slit was provided on anode side (inlet 2) for introducing inflow 2 into the reactor. A spacer (both sides adhesive tape, 20 μm thickness, Nitto Denko) was used to leave a rectangular channel exposed, and the two plates were simply sandwiched together. After connecting Teflon tubing to inlets and outlet, the reactor was sealed with epoxy resin. The dimensions of the channel were 1 cm width, 20 μm depth, and 6 cm total length and area of the two electrodes was 3 cm^2.

General procedure for preparative electrolysis

KdScientific model 100 syringe pumps were used to pump the reaction solutions. Two solutions were flowed through a cooling bath (0 °C) before introducing into the reactor. All reactions were conducted galvanostatically. Conditions of the cathodic cross-coupling reaction between **1a** and **2a** in the microreactor are described in the footnote *a* of Table 1 in the main text. The reaction mixture was analyzed by GC. For isolation of the products, the reaction mixture (5 mL) was added to a 50 mL of water and the aqueous layer was extracted three times with a 30 mL of diethyl ether. The combined organic fractions were washed with brine, dried over Na_2SO_4 and concentrated *in vacuo*. The residue was purified by column chromatography on silica gel with hexane–AcOEt. ^{1}H NMR yields of the crude mixture was determined with an internal standard ($MeNO_2$). All products except for **4b** were identified by authentic samples and literatures (**3a**,[9] **4a**,[9] **3b**,[20] **3c**,[21] **4c**,[22] **3d**,[21] **4d**,[23] **3e** [9] and **4e** [9]) using ^{1}H NMR and mass spectroscopy. Compound **4b** was identified by using ^{1}H and ^{13}C NMR, IR, mass, and high-resolution mass spectroscopy.

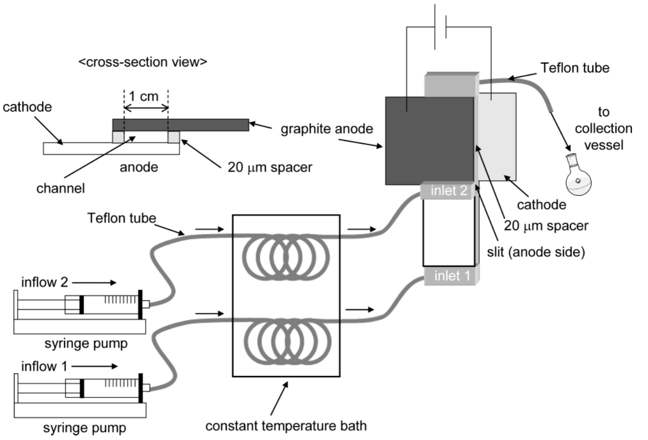

Fig. 12 Schematic illustration of the microreactor system.

2,2-Dimethyl-1-phenyl-but-3-en-1-ol (3a). Colorless oil; ^{1}H NMR (270 MHz, $CDCl_3$): δ 7.29 (s, 5H), 5.92 (dd, J = 17.3, 10.5 Hz, 1H), 5.16–5.04 (m, 2H), 4.43 (s, 1H), 1.02 (s, 3H), 0.96 (s, 3H); MS (EI) m/z (relative intensity): 176 ([M$^+$], 0.26), 107 (100), 79 (93), 70 (98).

4-Methyl-1-phenyl-pent-3-en-1-ol (4a). Colorless oil; ^{1}H NMR (270 MHz, $CDCl_3$): δ 7.40–7.23 (m, 5H), 5.20–5.14 (m, 1H), 4.68 (dd, J = 8.1, 5.7 Hz, 1H), 2.55–2.38 (m, 2H), 1.83 (bs, 1H), 1.72 (s, 3H), 1.61(s, 3H); MS (EI) m/z (relative intensity): 176 ([M$^+$], 4.3), 107 (99), 79 (95), 70 (100).

2,2-Dimethyl-1-(4-trifluoromethyl-phenyl)-but-3-en-1-ol (3b). Colorless oil; ^{1}H NMR (270 MHz, $CDCl_3$): δ 7.56 (d, J = 8.1 Hz, 2H), 7.41 (d, J = 8.1 Hz, 2H), 5.88 (dd, J = 17.6, 10.8 Hz, 1H), 5.20–5.05 (m, 2H), 4.48 (s, 1H), 2.11 (bs, 1H), 1.02 (s, 3H), 0.96 (s, 3H); MS (EI) m/z (relative intensity): 244 ([M$^+$], 0.01), 225 (9), 175 (98), 147 (33), 127 (88), 70 (100).

4-Methyl-1-(4-trifluoromethyl-phenyl)-pent-3-en-1-ol (4b). Colorless oil; IR (neat NaCl, ν/cm^{-1} 3370, 2920, 1620, 1420, 1330, 1170, 1130, 1070, 1020, 890; ^{1}H NMR (270 MHz, $CDCl_3$): δ 7.60 (d, J = 8.10 Hz, 2H), 7.48 (d, J = 8.10 Hz, 2H), 5.18–5.12 (m, 1H), 4.75 (t, J = 5.67, 1H), 2.48–2.42 (m, 2H), 2.08 (bs, 1H), 1.74 (s, 3H), 1.61 (s, 3H); ^{13}C NMR (67.8 MHz, $CDCl_3$): δ 148.00, 136.45, 125.95, 125.11 (q, J = 3.9 Hz), 118.85, 73.31, 38.37, 25.94, 18.01; MS (EI) m/z (relative intensity): 244 ([M$^+$], 0.09), 225 (3), 175 (62), 147 (10), 127 (49), 70 (100); HRMS (EI) m/z calcd. for $C_{13}H_{13}F_3O$ $[M^+–2H]$: 242.0913, found: 242.0912.

2,2-Dimethyl-1-naphthalen-2-yl-but-3-en-1-ol (3c). Pale yellow oil; ^{1}H NMR (270 MHz, $CDCl_3$): δ 7.84–7.74 (m, 4H), 7.48–7.42 (m, 3H), 5.97 (dd, J = 17.6, 10.8 Hz, 1H), 5.18–5.06 (m, 2H), 4.60 (s, 1H), 2.14 (bs, 1H), 1.06 (s, 3H), 1.01 (s, 3H); MS (EI) m/z (relative intensity): 226 ($[M^+]$, 4.6), 157 (100), 129 (92), 102 (3), 77 (6).

4-Methyl-1-naphthalen-2-yl-pent-3-en-1-ol (4c). Pale yellow oil; ^{1}H NMR (270 MHz, $CDCl_3$): δ 7.84–7.81 (m, 4H), 7.51–7.42 (m, 3H), 5.23–5.16 (m, 1H), 4.85 (dd, J = 7.6, 5.4 Hz, 1H), 2.58–2.51 (m, 2H), 2.11 (bs, 1H), 1.73 (s, 3H), 1.63 (s, 3H); MS (EI) m/z (relative intensity): 226 ($[M^+]$, 5.1), 208 (12), 193 (21), 178 (16), 157 (100), 129 (96), 115 (4), 89 (5), 77 (6).

2,2-Dimethyl-1-*p*-tolyl-but-3-en-1-ol (3d). Colorless oil; ^{1}H NMR (270 MHz, $CDCl_3$): δ 7.20–7.10 (m, 4H), 5.92 (dd, J = 17.5, 10.9 Hz, 1H), 5.15–5.04 (m, 2H), 4.40 (s, 1H), 2.34 (s, 3H), 1.01 (s, 3H), 0.95 (s, 3H); MS (EI) m/z (relative intensity): 190 ($[M^+]$, 0.29), 121 (100), 93 (81), 77 (64), 70 (69).

4-Methyl-1-*p*-tolyl-pent-3-en-1-ol (4d). Colorless oil; ^{1}H NMR (270 MHz, $CDCl_3$): δ 7.25 (d, J = 8.07 Hz, 2H), 7.15 (d, J = 8.07 Hz, 2H), 5.20–5.14 (m, 1H), 4.64 (dd, J = 7.91 Hz, 5.27, 1H), 2.58–2.29 (m, 2H), 2.34 (s, 3H), 1.94 (bs, 1H), 1.73 (s, 3H), 1.62 (s, 3H); MS (EI) m/z (relative intensity): 190 ($[M^+]$, 1.3), 172 (10), 157 (16), 142 (11), 121 (100), 93 (80), 77 (57), 70 (58).

1-Furan-3-yl-2,2-dimethyl-but-3-en-1-ol (3e). Yellow oil; ^{1}H NMR (270 MHz, $CDCl_3$): δ 7.36–7.7.34 (m, 2H), 6.37–6.36 (m, 1H), 5.91 (dd, J = 17.3, 10.8 Hz, 1H), 5.17–5.07 (m, 2H), 4.40 (s, 1H), 1.03 (s, 3H), 1.00 (s, 3H); MS (EI) m/z (relative intensity): 166 ($[M^+, 8]$), 133 (1), 97 (100), 70 (90).

1-Furan-3-yl-4-methyl-pent-3-en-1-ol (4e). Yellow oil; ^{1}H NMR (270 MHz, $CDCl_3$): δ 7.39–7.37 (m, 2H), 6.42–6.41 (m, 1H), 5.20–5.12 (m, 1H), 4.66 (dd, J = 7.26, 5.79 Hz, 1H), 2.55–2.37 (m, 2H), 1.85 (bs, 1H), 1.73 (s, 3H), 1.65 (s, 3H); MS (EI) m/z (relative intensity): 166 ($[M^+]$, 10.9), 148 (4.4), 133 (3.5), 119 (4.1), 97 (100), 70 (95).

CFD simulation settings

A T-type planer (2D) geometry and boundary conditions used are shown in Fig. 13. The quadrilateral mesh was generated by using the pre-processor Gambit 2.4 software (ANSYS Inc.). The physical properties and simulation parameters used in the present work are listed in Table 3. A uniform inlet velocity was set at the two inlets and input streams were assumed to develop into laminar flows. In application of Fluent 6.3, Navier–Stokes equations and species transport equations were solved simultaneously. No heat transfer and no reaction between transported species were presumed. A no-slip boundary condition was used at the walls where the velocity is zero.

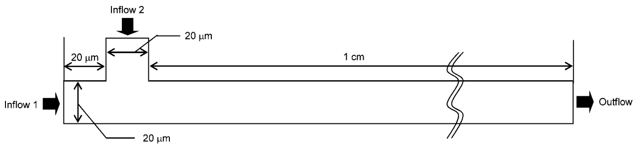

Fig. 13 Schematic illustration of the geometry and the boundary conditions used in the CFD simulation.

Table 3 Simulation settings and physical properties of liquids used for the simulations

Property	Value
Mesh number	1 046 000
Inlet velocity (Inflow 1 and Inflow 2)	8.33×10^{-4} m s^{-1}
Mass fraction of benzaldehyde (Inflow 1)	0
Mass fraction of benzaldehyde (Inflow 2)	0.206
Molecular weight (HMPA)	179.2 kg kmol^{-1}
Molecular weight (benzaldehyde)	106.12 kg kmol^{-1}
Density (HMPA)	1030 kg m^{-3}
Density (benzaldehyde)	1041.5 kg m^{-3}
Dynamic viscosity[a]	1.11×10^{-2} Pa s

[a] Obtained by rheology measurements of Fig. 5.

Acknowledgements

This work was financially supported in part by the Global COE Program (Tokyo Institute of Technology, Education and Research Center for Emergence of New Molecular Chemistry) and a Grant-in-Aid for JSPS Fellows from the Japanese Ministry of Education, Culture, Sports, Science and Technology.

Notes and references

1 (*a*) K. Matsuda, M. Atobe and T. Nonaka, *Chem. Lett.*, 1994, 1619; (*b*) M. Atobe and T. Nonaka, *Chem. Lett.*, 1995, 669; (*c*) M. Atobe, K. Matsuda and T. Nonaka, *Electroanalysis*, 1996, **8**, 784; (*d*) M Atobe and T. Nonaka, *J. Electroanal. Chem.*, 1997, **425**, 161.

2 M. Iannelli, V. Alupei and H. Ritter, *Tetrahedron*, 2005, **61**, 1509.

3 (*a*) B. J. Cohen, M. A. Kraus and A. Patchornik, *J. Am. Chem. Soc.*, 1977, **99**, 4165; (*b*) B. Helms, S. J. Guillaudeu, Y. Xie, M. McMurdo, C. J. Hawker and J. M. J. Fréchet, *Angew. Chem., Int. Ed.*, 2005, **44**, 6384; (*c*) T. Tajima and A. Nakajima, *J. Am. Chem. Soc.*, 2008, **130**, 10496.

4 (*a*) G. Jas and A. Kirschning, *Chem.–Eur. J.*, 2003, **9**, 5708; (*b*) S. Suga, A. Nagaki and J. Yoshida, *Chem. Commun.*, 2003, 354; (*c*) A. Nagaki, H. Kim and J. Yoshida, *Angew. Chem., Int. Ed.*, 2009, **48**, 8063; (*d*) D. Webb and T. F. Jamison, *Chem. Sci.*, 2010, **1**, 675.

5 For selected books and reviews on microreactor technology, see: (*a*) *Microreaction Technology*, ed. W. Ehrfeld, Springer, Berlin, 1998; (*b*) S. J. Haswell, P. D. I. Fletcher, G. M. Greenway, V. Skelton, P. Styring, D. O. Morgan, S. Y. F. Wong and B. H. Warrington, in *Automated Synthetic Methods for Speciality Chemicals*, ed. W. Hoyle, Royal Society of Chemistry, Cambridge, 1999, p. 26; (*c*) *Microsystem Technology in Chemistry and Life Sciences*, ed. A. Manz and H. Becker, Springer, Berlin, 1999; (*d*) *Microreactors*, ed. W. Ehrfeld, V. Hessel and H. Löwe, Wiley-VCH, Weinheim, 2000; (*e*) K. F. Jensen, *Chem. Eng. Sci.*, 2001, **56**, 293; (*f*) S. J. Haswell, R. J. Middleton, B. O'Sullivan, V. Skelton, P. Watts and P. Styring, *Chem. Commun.*, 2001, 391; (*g*) P. D. I. Fletcher, S. J. Haswell, E. Pombo-Villar, B. H. Warrington, P. Watts, S. Y. F. Wong and X. Zhang, *Tetrahedron*, 2002, **58**, 4735; (*h*) K. Jähnisch, V. Hessel and H. Löwe, *Angew. Chem., Int. Ed.*, 2004, **43**, 406; (*i*) J. Yoshida, A. Nagaki, T. Iwasaki and S. Suga, *Chem. Eng. Technol.*, 2005, **28**, 259; (*j*) K. Geyer, J. D. C. Codée and P. H. Seeberger, *Chem.–Eur. J.*, 2006, **12**, 8434; (*k*) A. J. deMello, *Nature*, 2006, **442**, 394; (*l*) B. P. Mason, K. E. Price, J. L. Steinbacher, A. R. Bogdan and D. T. McQuade, *Chem. Rev.*, 2007, **107**, 2300; (*m*) J. Yoshida and S. Suga, *Electrochemistry*, 2007, **75**, 58; (*n*) J. Yoshida, A. Nagaki and T. Yamada, *Chem.–Eur. J.*, 2008, **14**, 7450; (*o*) T. Fukuyama, Md. T. Rahman, M. Sato and I. Ryu, *Synlett*, 2008, **2**, 151; (*p*) F. E. Valera, M. Quaranta, A. Moran, J. Blacker, A. Armstrong, J. T. Cabral and D. G. Blackmond, *Angew. Chem., Int. Ed.*, 2010, **49**, 2478.

6 S. Suga, D. Yamada and J. Yoshida, *Chem. Lett.*, 2010, **39**, 404.

7 F. Amemiya, K. Fuse, T. Fuchigami and M. Atobe, *Chem. Commun.*, 2010, **46**, 2730.

8 (*a*) M. M. Baizer and J. L. Chruma, *J. Org. Chem.*, 1972, **37**, 1951; (*b*) S. Satoh, H. Suginome and M. Tokuda, *Bull. Chem. Soc. Jpn.*, 1981, **54**, 3456; (*c*) S. Satoh, H. Suginome and M. Tokuda, *Bull. Chem. Soc. Jpn.*, 1983, **56**, 1791; (*d*) K. Uneyama, H. Matsuda and S. Torii, *Tetrahedron Lett.*, 1984, **25**, 6017; (*e*) S. Sibille, E. d'Incan, L. Laport and J. Perichon, *Tetrahedron Lett.*, 1986, **27**, 3129.

9 M. Tokuda, S. Satoh and H. Suginome, *J. Org. Chem.*, 1989, **54**, 5608.

10 (*a*) S. Rondinini, P. R. Mussini, P. Mutini and G. Sello, *Electrochim. Acta*, 2001, **46**, 3245; (*b*) J. Simonet, *J. Electroanal. Chem.*, 2005, **583**, 34; (*c*) C. Bellomunno, D. Bonanomi, L. Falciola, M. Longhi, P. R. Musini, L. M. Doubova and G. D. Silvestro, *Electrochim. Acta*, 2005, **50**, 2331; (*d*) A. A. Isse, S. Gotardello, C. Maccato and A. Gennaro, *Electrochem. Commun.*, 2006, **8**, 1707.

11 G. J. Janz and R. P. T. Tomkins, in *Nonaqueous Electrolytes Handbook*, Academic Press, Now York, 1972, vol. I, p. 5.

12 A. M. Bond, E. A. Mclennan, R. S. Stojanovic and F. G. Thomas, *Anal. Chem.*, 1987, **59**, 2853.

13 (*a*) P. A. Z. Suarez, S. Einloft, J. E. L. Dullius, R. F. de Souza and J. Dupont, *J. Chim. Phys. Phys.-Chim. Biol.*, 1998, **95**, 1626; (*b*) V. M. Hultgren, A. W. A. Mariotti, A. M. Bond and A. G. Wedd, *Anal. Chem.*, 2002, **74**, 3151.

14 U. Schröder, J. D. Wadhawan, R. G. Compton, F. Marken, P. A. Z. Suarez, C. S. Consorti, R. F. de Souza and J. Dupont, *New J. Chem.*, 2000, **24**, 1009.

15 (*a*) C. R. Wilke and P. Chang, *AIChE J.*, 1955, **1**, 264; (*b*) J. C. Giddings, in *Dynamics of Chromatography, Part I, Principles and Theory*, Marcel Dekker, New York, 1965; (*c*) R. C. Reid, J. M. Prausnitz and T. K. Sherwood, in *The Properties of Gases and Liquids*, McGraw-Hill, New York, 3rd edn, 1977, p. 567; (*d*) R. E. Treybal, in *Mass-transfer Operations*, McGraw-Hill, New York, 1980; (*e*) D. M. Ruthven, in *Principles of Adsorption & Adsorption Processes*, John Wiley and Sons, New York, 1984; (*f*) M. Suzuki, in *Adsorption Engineering*, Kodansha/Elsevier, Tokyo/Amsterdam, 1990; (*g*) G. Guiochon, S. Golshan-Shirazi and A. M. Katti, in *Fundamentals of Preparative and Nonlinear Chromatography*, Academic Press, Boston, 1994; (*h*) R. B. Bird, W. E. Stewart and E. N. Lightfoot, in *Transport Phenomena*, John Wiley & Sons, New York, 2002.

16 R. C. Reid, J. M. Prausnitz and T. K. Sherwood, in *The Properties of Gases and Liquids*, McGraw-Hill, New York, 3rd edn, 1977, p. 57.

17 (*a*) K. Gast, G. Damaschun, R. Misselwitz and D. Zirwer, *Eur. Biophys. J.*, 1992, **21**, 357; (*b*) G. Damaschun, H. Damaschun, K. Gast and D. Zirwer, *J. Mol. Biol.*, 1999, **291**, 715.

18 (*a*) M. Liu, J. K. Nicholson, J. A. Parkinson and J. C. Lindon, *Anal. Chem.*, 1997, **69**, 1504; (*b*) K. F. Morris, B. J. Cutak, A. M. Dixon and C. K. Larive, *Anal. Chem.*, 1999, **71**, 5315.

19 K. Pappaert, J. Biesemans, D. Clicq, S. Vankrunkelsven and G. Desmet, *Lab Chip*, 2005, **5**, 1104.

20 H. S. Schrekker, M. W. G. de Bolster, R. V. A. Orru and L. A. Wessjohann, *J. Org. Chem.*, 2002, **67**, 1975.

21 H-. M. Chang and C-. H. Cheng, *Org. Lett.*, 2000, **2**, 3439.

22 H-. S. Cheng and T-. P. Loh, *J. Am. Chem. Soc.*, 2003, **125**, 4990.

23 Y. Kusuyama, *Bull. Chem. Soc. Jpn.*, 1998, **71**, 685.